JOURNAL OF GEOPHYSICAL RESEARCH, VOL. 104, NO. D7, PAGES 8263–8280, APRIL 20, 1999

Ozone profiles from GOME satellite data: Algorithm description and first validation

Ricarda Hoogen, Vladimir V. Rozanov, and John P. Burrows
Institut für Umweltphysik, Universität Bremen, Germany

Abstract. In April 1995 the Global Ozone Monitoring Experiment (GOME) was launched aboard the European Space Agency's second European Remote Sensing (ERS-2) satellite. GOME is a nadir-viewing spectrometer measuring solar radiation backscattered by the system Earth-atmosphere in the ultraviolet and visible spectral range. For the retrieval of ozone vertical distributions from GOME measurements the Full Retrieval Method (FURM) has been developed. It is based on the optimal estimation approach and on results from information theory. The joint retrieval of the ozone profile and several additional parameters (e.g., surface albedo) enables the ozone profile retrieval to be extended below the ozone number density maximum. A first validation of the GOME profiles is performed by a comparison with approximately 200 coincident ozonesonde measurements from five European stations. The RMS difference between ozone subcolumn amounts in 10 km layers as measured by GOME and by the sondes is approximately 7-8 % in the middle stratosphere and 15-20 % in the lower stratosphere. Furthermore, it is demonstrated that information about the ozone content in the troposphere can be retrieved from the GOME measurements.

1. Introduction

The concern about the anthropogenic impact on the ozone layer dramatically increased after the discovery of the Antarctic ozone hole in the early 1980s, which at that time was completely unexpected [*Farman et al.*, 1985]. This has led to an unprecedented scientific effort in the subsequent years to improve our understanding about the natural and anthropogenic influences on the stratospheric ozone layer. As a result, our knowledge of atmospheric dynamics, photochemistry, heterogeneous and homogeneous chemistry has increased significantly. More recently, tropospheric ozone distributions, in particular enhanced ozone concentrations resulting from summer smog events in industrialized regions and from biomass burning in the tropics, have become a topic of great scientific interest [e.g., *Fishman et al.*, 1990, 1996; *Suhre et al.*, 1997].

Although measurements of total ozone columns are of great importance, they are insufficient to gain a thorough understanding of the chemical and dynamical processes determining the ozone variations. Height-resolved ozone information on a global scale over an extended period of time and having reasonable temporal and spatial resolution is needed. In this context, the Global Ozone Monitoring Experiment (GOME) on the European Space Agency's second European Remote Sensing (ERS-2) satellite is intended to make an important contribution. GOME is a small-scale version of the Scanning Imaging Absorption Spectrometer for Atmospheric Chartography (SCIAMACHY) to be launched on the ENVISAT-1 (first Environmental Satellite) platform in the year 2000 [*Burrows et al.*, 1991, 1995, 1999b]. It is a nadir-viewing spectrometer measuring the solar radiation backscattered by the atmosphere and the Earth surface in the ultraviolet and visible spectral range.

The idea of deriving ozone vertical distributions from nadir measurements of backscattered ultraviolet radiation goes back to *Singer and Wentworth* [1957]. Its first sucessful realization, the Backscatter Ultraviolet (BUV) instrument on NASA's Nimbus-4 satellite launched in 1970 [*Heath et al.*, 1973], was continued by the Solar Backscatter Ultraviolet (SBUV) experiment on Nimbus-7 [*Heath et al.*, 1975], the follow-on SBUV/2 instruments flown on the NOAA polar satellites, and the SSBUV instrument designed for missions on the space shuttle [*Hilsenrath et al.*, 1988]. These instruments measure backscattered ultraviolet radiances at 12 wavelengths between 252 and 340 nm with approximately 1.1 nm bandwidth. Starting from an early algorithm by *Mateer et al.* [1971], NASA's Ozone Processing Team (OPT) has developed several versions of the algorithm used to process measurements from the BUV instruments [*Bhartia et al.*, 1996, and references therein].

The GOME instrument observes the entire wavelength range between 240 and 790 nm with a spectral

Paper number 1998JD100093.
0148-0227/99/1998JD100093$09.00

resolution of 0.2-0.3 nm. Thus it provides more information about the temperature dependent Huggins bands and the relatively temperature independent Chappuis bands of ozone than the above instruments. This, coupled with the high signal-to-noise ratio of GOME, implies some potential for extending the retrieval of ozone information below the ozone maximum.

In this paper a brief overview of the main features of the GOME instrument is given, followed by a description of the forward model GOMETRAN used for the calculation of radiances and weighting functions needed for the retrieval of ozone profiles from GOME spectra. Next, the inverse method and its implementation in the Full Retrieval Method (FURM) algorithm are presented. This includes a discussion of the information content of the measurements and of the vertical resolution of the retrieved profiles. Finally, the first validation of GOME ozone profiles derived with the FURM algorithm is undertaken by comparison with ozonesonde measurements.

2. Instrument GOME

On April 20, 1995, GOME was launched aboard the European Space Agency's ERS-2 satellite from Kourou, French Guyana. ERS-2 is operated in a near-polar Sun-synchronous orbit having a mean altitude of 785 km and an orbital period of 100 min. The satellite moves at a velocity of 7 km/s over ground and crosses the equator on the descending node at approximately 1030 LT.

After a series of function and performance tests routine measurements started on July 1, 1995. On the illuminated part of the orbit, GOME performs nadir observations of the Earth by scanning across track from east to west. The current scan amplitude is $\pm 30°$ corresponding to a swath width of 960 km. With this swath, global coverage is achieved within 3 days (43 orbits) at the equator and less than 3 days at higher latitudes. One complete scan cycle takes 6 s, comprising three 1.5 s forward scans and a 1.5 s backscan. On the night side of the orbit, a variety of calibration measurements are performed.

GOME is a multichannel spectrometer covering the wavelength range from 240 to 790 nm with a spectral resolution of 0.2-0.3 nm. In nadir-viewing mode the light enters the instrument via the nadir scan mirror and is focused on the entrance slit of the spectrometer by an anamorphous telescope formed by two cylindrical mirrors. The instantaneous field of view is $2.9° \times 0.14°$, corresponding to an area of $40 \times 2\,\mathrm{km}^2$ on the ground (with the longer dimension parallel to the flight direction). By means of a predisperser prism, a channel separator, and a beam splitter the light beam is split into four spectral bands. Each of the four bands is dispersed by a diffraction grating and focused on a Peltier-cooled silicon diode array detector consisting of 1024 individual detector pixels. The whole spectrum is recorded simultaneously; that is, no spectral scans are performed.

Table 1. Spectral Coverage, Spectral Resolution, and Integration Time of the GOME Spectral Channels

Channel	Coverage, nm	Resolution, nm	Int. Time, s
1A	238–307	0.2	12.0
1B	307–314	0.2	1.5
2	311–404	0.3	1.5
3	394–611	0.3	1.5
4	578–794	0.3	1.5

To optimize the signal-to-noise ratio in the UV region of the spectrum, where the dynamic range of the measurement signal spans several orders of magnitude, the channel-1 diode array is divided into two virtual bands, 1A and 1B, which can be programmed to different integration times. For band 1A an integration time of 12 s was selected. During this time GOME performs two complete scan cycles, which corresponds to a ground pixel size of $960 \times 100\,\mathrm{km}^2$ (across track $\times$ along track). The integration time in band 1B and in channels 2 to 4 is 1.5 s, leading to a ground pixel size of $320 \times 40\,\mathrm{km}^2$ for the forward scan pixels and of $960 \times 40\,\mathrm{km}^2$ for the backscan pixels. The spectral coverage and resolution as well as the integration times of the four channels are listed in Table 1.

To correct accurately for the polarization sensitivity of the GOME instrument, the actual degree of polarization of the incoming light has to be determined. For this purpose, a small fraction of light polarized perpendicular to the main optical plane is reflected off the predisperser prism toward three dedicated Polarization Measurement Devices (PMDs), which are broadband silicon diodes covering approximately the spectral ranges 300-400 nm, 400-600 nm, and 600-800 nm. The PMDs are read out every 93.75 ms, which corresponds to an area of $20 \times 40\,\mathrm{km}^2$ on the ground (across track $\times$ along track). Their relatively good horizontal resolution makes the PMDs a valuable tool for cloud detection.

To exclude effects of solar variations on the derivation of atmospheric parameters from earthshine spectra, it is common practice to normalize the earthshine radiance to the solar irradiance. For this purpose, GOME performs daily measurements of the direct solar irradiance via a Sun view mirror and a Sun diffusor. From the diffusor the solar beam is directed to the nadir scan mirror beyond which the optical path is identical to the one followed by the earthshine radiation. Therefore instrument changes in the common optical path cancel to a large extent in the Sun-normalized radiance.

Instrument functions needed for the radiometric calibration of the GOME spectra, i.e., the bidirectional reflection distribution function of the diffusor, the polarization sensitivity function, and the radiance and irradiance response functions of GOME, were determined during the preflight calibration. Long-term monitoring of the instrument performance and the periodic update of the inflight calibration are essential for the data quality. In-orbit spectral calibration measurements are per-

formed on a monthly basis using an internal Pt/Cr/Ne hollow cathode discharge lamp. More detailed information on the GOME instrument and operation can be found in the GOME users manual [*European Space Agency,* 1995].

The work presented in this paper is based on the operational GOME level-1 data product, i.e., on geolocated, spectrally and radiometrically calibrated earthshine radiances and solar irradiances. The conversion of raw measurements (level-0 data) to level-1 data is performed with the GOME Data Processor (GDP) installed at the German Remote Sensing Data Center (DFD) of the Deutsche Forschungsanstalt für Luft- und Raumfahrt (DLR), which is part of the official Data Processing and Archiving Facility (D-PAF) of GOME. For details of the level-0 to level-1 processor the reader is referred to the algorithm description [*Deutsche Forschungsanstalt für Luft- und Raumfahrt,* 1996].

3. Forward Model GOMETRAN

For the retrieval of ozone profiles from GOME data a fast and accurate radiative transfer model (RTM) for the calculation of earthshine radiances and weighting functions is essential. The RTM GOMETRAN was specifically designed for the evaluation of GOME data, without however being restricted to this application [*Rozanov et al.,* 1997]. It solves the scalar radiative transfer equation using the finite differences method. It is a monochromatic model and includes full multiple-scattering treatment. To account for the curvature of the atmosphere, the direct radiation component is treated in spherical geometry.

In retrieval theory the weighting functions, which describe the response of the radiance to small deviations of the atmospheric parameters from a given atmospheric state, are of particular importance. In mathematical terms the weighting functions are partial derivatives of the forward model with respect to the atmospheric parameters. These derivatives are usually calculated by means of numerical perturbation schemes. The finite differences method allows the direct, quasi-analytical computation of the weighting functions, which drastically reduces the computation time [*Rozanov et al.,* 1998].

In GOMETRAN the geometrical height is used as the vertical coordinate. To ensure accurate RT calculations, the atmosphere is divided into 80 equidistant layers between 0 and 80 km altitude. For ground heights above sea level the layering is appropriately adjusted.

The NO_2 and ozone absorption cross sections used in this work were measured in the laboratory with the GOME flight model and therefore already contain the instrument slit function [*Burrows et al.,* 1998, 1999a]. In order to derive the temperature dependence of the cross sections, the measurements were performed at a broad range of atmospheric temperatures. In GOMETRAN, at each height level the absorption cross sections for the associated temperature are used. Temperature and pressure profiles are derived from analyses of the National Meteorological Center (NMC) for the respective day and geolocation. The Rayleigh scattering cross sections and phase functions are based on the work of *Bucholtz* [1995]. The wavelength dependent anisotropy factors are taken from *Bates* [1984]. Aerosol profiles and optical properties are taken from the LOWTRAN-7 aerosol model [*Kneizys et al.,* 1988]. The Earth surface is assumed to be a Lambertian reflector with wavelength dependent albedo. The surface information is extracted from a global data base compiled by R. Guzzi (private communication, 1997). This data set provides the ground height and the surface type (discriminating between sand, soil, snow, vegetation, and water) at a spatial resolution of $1° \times 1°$. In addition, for each surface type the albedo is given in the spectral range from 240 to 800 nm. Clouds can be described either as scattering layers of cloud droplets or as bidirectionally reflecting surfaces inserted into the model atmosphere at an altitude corresponding to the cloud top height [*Kurosu et al.,* 1997].

4. Inverse Model FURM

The inverse method used to derive ozone profiles from GOME measurements is based on the well-known optimal estimation approach. To enhance the performance of this method, results from information theory are explicitly taken into account. In this section the theoretical background of this improved optimal estimation scheme and its implementation in the FURM algorithm are presented. The discussion of the weighting functions is intended to provide some insight into the information actually retrievable from the GOME measurements. Furthermore, the question of vertical resolution and retrieval errors is addressed.

4.1. Retrieval Method

The retrieval of ozone profiles from GOME data is an underconstrained problem for the trivial reason that the ozone profile is a continuous function of altitude, whereas GOME provides measurements only at a limited number of wavelengths. In order to numerically solve the inverse problem, the ozone profile is discretized to a finite number of height levels between which it is assumed to be a linear function of altitude. To avoid unnecessary interpolations, in the FURM code the altitude grid used for the inversion is identical to the one used for the forward calculations.

The inverse problem is also underconstrained because there are components in the actual ozone profile which do not contribute to the measurements and, consequently, cannot be determined from them. Thus additional information is needed to retrieve a physically reasonable solution. For many regions of the world there already exists a considerable number of ozone profile measurements performed by various in situ and remote

sensing techniques. These measurements can be statistically evaluated and used as a priori knowledge about typical ozone distributions. This is independent information which constrains the retrieval solution. This approach is used in the optimal estimation method, which was selected as the basic retrieval method in the FURM algorithm.

Since the radiance is a nonlinear function of the atmospheric parameters, the retrieval solution has to be found iteratively. In the iteration step $i+1$ the optimal estimation solution can be written as [*Rodgers,* 1976]

$$\mathbf{x}_{i+1} = \mathbf{x}_a + (\mathbf{K}_i^T \mathbf{S}_\mathbf{y}^{-1} \mathbf{K}_i + \mathbf{S}_a^{-1})^{-1} \mathbf{K}_i^T \mathbf{S}_\mathbf{y}^{-1} \cdot [\mathbf{y} - \mathbf{y}_i + \mathbf{K}_i(\mathbf{x}_i - \mathbf{x}_a)], \quad (1)$$

where $\mathbf{y}$ is the measurement vector, $\mathbf{y}_i$ is the same quantity calculated with the forward model using the result $\mathbf{x}_i$ from the previous iteration, $\mathbf{S}_\mathbf{y}$ is the measurement error covariance matrix, $\mathbf{S}_a$ is the a priori covariance matrix, $\mathbf{x}_a$ is the a priori atmospheric state, and $\mathbf{K}_i$ is the weighting function matrix after the ith iteration. The superscripts T and -1 designate the matrix transpose and inverse, respectively. After convergence has occurred, the result of the last iteration is identified with the retrieval solution $\hat{\mathbf{x}}$. The corresponding solution covariance matrix is given by [*Rodgers,* 1976]

$$\hat{\mathbf{S}} = (\hat{\mathbf{K}}^T \mathbf{S}_\mathbf{y}^{-1} \hat{\mathbf{K}} + \mathbf{S}_a^{-1})^{-1}. \quad (2)$$

$\hat{\mathbf{S}}$ is the sum of the covariance matrix $\hat{\mathbf{S}}_n$, describing the error due to measurement noise, and of the covariance matrix $\hat{\mathbf{S}}_s$, describing the so-called smoothing error caused by the use of a priori information. Explicit expressions for $\hat{\mathbf{S}}_n$ and $\hat{\mathbf{S}}_s$ can be found in the work of *Rodgers* [1990].

In the FURM algorithm the measurement vector $\mathbf{y}$ is defined as the logarithm of the Sun-normalized radiance. Correspondingly, the diagonal elements of the measurement error covariance matrix $\mathbf{S}_\mathbf{y}$ are the squares of the relative random errors of the Sun-normalized radiances. The off-diagonal elements are set to zero; that is, the measurement errors at different wavelengths are assumed to be uncorrelated. For the retrievals presented in this paper, $\mathbf{y}$ typically contains 580-590 elements.

The a priori ozone profiles used in this work are taken from a global ozone climatology based on ozonesonde and satellite measurements [*Fortuin and Kelder,* 1999]. This climatology provides monthly zonal mean ozone profiles for 10° wide latitude bands covering the pressure range from 1000 to 0.3 hPa. The variances of the ozone distributions, i.e., the diagonal elements of $\mathbf{S}_a$, are derived from the predecessor climatology, which is based on ozonesonde measurements only [*Fortuin,* 1996]. This climatology has the same temporal and latitude resolution as the above mentioned climatology. The covariances are approximated by

$$S_{a,kl} = \sigma_{a,k}\sigma_{a,l} \exp(-|z_k - z_l|/r_c), \quad (3)$$

where z_k is the kth altitude level, $\sigma_{a,k}^2$ is the corresponding variance, and r_c is the correlation length, which was assumed to be 5 km over the whole atmosphere.

The radiance in the UV-visible spectral range is not only influenced by ozone absorption but also by several other atmospheric parameters not known a priori with sufficient accuracy. These parameters are therefore taken into account as additional fit parameters in the FURM algorithm. From studies with real and simulated spectra it was found that by including the following additional parameters in the state vector $\mathbf{x}$, the ozone profile results can be considerably improved: a scaling factor for the surface albedo, a scaling factor for the aerosol number density profile, a scaling factor for the NO_2 number density profile, a scaling factor for the pressure profile, and a shift parameter for the temperature profile.

Adding these "scalar" fit parameters to the ozone profile leads to a state vector of typically 80-85 elements. This number is much larger than the rank of the weighting function matrix $\mathbf{K}$ formally defining the maximum number of independent parameters that can be retrieved from the measurement. In the presence of measurement noise the number of parameters measured to useful accuracy may even be smaller. It can be estimated by analyzing the information content of the measurement, which can be defined as the reduction in entropy of the posteriori knowledge about the atmospheric state with respect to the a priori knowledge [*Shannon and Weaver,* 1949]. By a priori and posteriori knowledge we understand the probability density functions describing the statistics of the atmospheric state before and after the measurement, $p_a(\mathbf{x})$ and $p_p(\mathbf{x})$, respectively. The entropy of a given probability density function $p(\mathbf{x})$ is given by

$$S(p) = -\int p(\mathbf{x}) \ln[p(\mathbf{x})/m(\mathbf{x})] d\mathbf{x}, \quad (4)$$

where $m(\mathbf{x})$ is an appropriate measure function and the integral is taken over the whole state space. The information content H of a measurement is then defined as

$$H = S(p_a) - S(p_p). \quad (5)$$

Under the assumption that the a priori information can be described by a Gaussian probability density function with expectation value $\mathbf{x}_a$ and covariance $\mathbf{S}_a$, the posteriori probability density function is also Gaussian with expectaction value $\hat{\mathbf{x}}$ and covariance $\hat{\mathbf{S}}$. In this case the information content can be shown to be [*Rodgers,* 1996]

$$H = \frac{1}{2} \ln[\det(\mathbf{S}_a)] - \frac{1}{2} \ln[\det(\hat{\mathbf{S}})]. \quad (6)$$

Using the abbreviation

$$\hat{\mathbf{P}} = \mathbf{S}_a \hat{\mathbf{G}} \quad \text{with} \quad \hat{\mathbf{G}} = \hat{\mathbf{K}}^T \mathbf{S}_\mathbf{y}^{-1} \hat{\mathbf{K}} \quad (7)$$

this can be rearranged to yield

$$H = \frac{1}{2} \ln[\det(\hat{\mathbf{P}} + \mathbf{I})] = \frac{1}{2} \sum_n \ln(\hat{\lambda}_n + 1), \quad (8)$$

where the $\hat{\lambda}_n$ are the eigenvalues of the matrix $\hat{\mathbf{P}}$. The matrix $\hat{\mathbf{P}}$ is positive definite; that is, its eigenvalues are all positive. Thus only eigenvalues $\hat{\lambda}_n > 1$ make a relevant contribution to the information content. The state space spanned by the associated eigenvectors corresponds to the effective state space accessible with the measurement.

An elegant way of adapting the number of fit parameters to the information content of the measurement was suggested by *Kozlov* [1983]. The principal idea is to expand the difference between $\mathbf{x}_{i+1}$ and $\mathbf{x}_a$ into a series of eigenvectors $\boldsymbol{\psi}_{i,n}$ of the matrix $\mathbf{P}_i$, which in the following is called Kozlov information matrix:

$$\mathbf{x}_{i+1} - \mathbf{x}_a = \sum_n \beta_{i,n} \boldsymbol{\psi}_{i,n}. \tag{9}$$

In this expansion, only eigenvectors with eigenvalues $\lambda_{i,n} > 1$ are taken into account. Now, instead of the state vector $\mathbf{x}_{i+1}$ itself, the expansion coefficients $\beta_{i,n}$ have to be determined. Inserting (9) in (1) yields

$$\sum_n \beta_{i,n} \boldsymbol{\alpha}_{i,n} + \sum_n \beta_{i,n} \mathbf{S}_a^{-1} \boldsymbol{\psi}_{i,n} = \mathbf{K}_i^T \mathbf{S}_\mathbf{y}^{-1} [\mathbf{y} - \mathbf{y}_i + \mathbf{K}_i (\mathbf{x}_i - \mathbf{x}_a)], \tag{10}$$

where the abbreviation

$$\boldsymbol{\alpha}_{i,n} = \mathbf{K}_i^T \mathbf{S}_\mathbf{y}^{-1} \mathbf{K}_i \boldsymbol{\psi}_{i,n} \tag{11}$$

was used. Like the $\boldsymbol{\psi}_{i,l}$, the $\boldsymbol{\alpha}_{i,n}$ form a basis of the state space. Since $\mathbf{P}_i$ is not symmetric, its eigenvectors $\boldsymbol{\psi}_{i,l}$ do not form an orthogonal basis. However, for the two basis sets the following biorthogonality relation holds:

$$\boldsymbol{\psi}_{i,l}^T \boldsymbol{\alpha}_{i,n} = \delta_{ln} N_{i,n}, \tag{12}$$

where δ_{ln} is the Kronecker delta. This relation can be proved as follows: $\boldsymbol{\psi}_{i,l}$ is a right eigenvector of $\mathbf{P}_i = \mathbf{S}_a \mathbf{G}_i$; that is, $\mathbf{S}_a \mathbf{G}_i \boldsymbol{\psi}_{i,l} = \lambda_{i,l} \boldsymbol{\psi}_{i,l}$. Multiplication of this eigenvalue equation with $\mathbf{G}_i$ yields $\mathbf{G}_i \mathbf{S}_a \mathbf{G}_i \boldsymbol{\psi}_{i,l} = \lambda_{i,l} \mathbf{G}_i \boldsymbol{\psi}_{i,l}$; that is, $\boldsymbol{\alpha}_{i,l} = \mathbf{G}_i \boldsymbol{\psi}_{i,l}$ is a right eigenvector of $\mathbf{G}_i \mathbf{S}_a$ and therefore a left eigenvector of $(\mathbf{G}_i \mathbf{S}_a)^T = \mathbf{P}_i$. Equation (12) then follows from the orthogonality of left and right eigenvectors.

From (7) and (11), and the eigenvalue equation for $\mathbf{P}_i$ the following expression can be derived:

$$\mathbf{S}_a^{-1} \boldsymbol{\psi}_{i,n} = \frac{1}{\lambda_{i,n}} \boldsymbol{\alpha}_{i,n}. \tag{13}$$

Multiplication of (10) with $\boldsymbol{\psi}_{i,l}^T$ and use of (12) and (13) finally yields an expression for the expansion coefficients $\beta_{i,n}$:

$$\beta_{i,n} = \frac{\lambda_{i,n}}{N_{i,n}(1 + \lambda_{i,n})} \cdot \boldsymbol{\psi}_{i,n}^T \mathbf{K}_i^T \mathbf{S}_\mathbf{y}^{-1} [\mathbf{y} - \mathbf{y}_i + \mathbf{K}_i (\mathbf{x}_i - \mathbf{x}_a)]. \tag{14}$$

This "eigenvector approach" uses a priori information in the same statistical sense as the original optimal estimation method. However, in the fit process, only those parameters are considered about which there is actually information contained in the measurement. Since only a small number of eigenvectors has to be calculated, this method is numerically very efficient and stable and therefore was adopted as the preferred method for ozone profile retrievals from GOME data.

Finally, it should be pointed out that for numerical reasons in the FURM algorithm the actual fit parameters are not the atmospheric parameters in absolute units but their relative deviations from the a priori values. This simply means, that in (1) the expression $\mathbf{x}_{i+1} - \mathbf{x}_a$ is replaced by $(\mathbf{x}_{i+1} - \mathbf{x}_a)/\mathbf{x}_a$. Accordingly, the a priori covariance matrix $\mathbf{S}_a$ is in relative units, and the weighting functions describe the response of the measurement to relative variations in the atmospheric parameters.

4.2. Shift-and-Squeeze Correction and Ring Effect

Unlike the earthshine radiance the solar irradiance measured by GOME is subject to a small Doppler shift due to the relative motion between the Sun and the satellite. This causes a shift between radiance and irradiance. In addition, GOME records the radiance and irradiance spectra at different positions in the orbit. Thus thermally induced shifts and possibly squeezes between the two spectra may occur. Since these shifts and squeezes can introduce artificial spectral structures in the Sun-normalized radiance, the two spectra have to be aligned by a suitable shift-and-squeeze routine before being ratioed. In the FURM algorithm the measured radiance serves as the spectral reference to which the irradiance, the simulated spectrum $\mathbf{y}_i$, and an appropriate Ring spectrum are aligned. The latter accounts for the so-called Ring effect, i.e., the filling-in of solar Fraunhofer lines first observed by *Shefov* [1959] and *Grainger and Ring* [1962]. The Ring effect can be explained to high accuracy by rotational Raman scattering (RRS) [*Vountas et al.*, 1998, and references therein]. Unfortunately, the simulation of RRS in a RTM is generally very timeconsuming. Therefore a data base of Ring spectra (defined as the logarithm of the ratio of the radiances with and without RRS, respectively) for various atmospheric scenarios and solar zenith angles was prepared using a dedicated version of GOMETRAN with RRS included. For each retrieval an appropriate Ring spectrum is selected from this data base and scaled with a Ring amplitude factor, which is determined in a prefit, before being subtracted from the measured Sun-normalized radiance.

4.3. Treatment of Cloudy Scenes

Estimates, based on the work of *Derrien* [1992], indicate that more than 99% of the GOME standard ground pixels ($320 \times 40\,\mathrm{km}^2$) are cloud contaminated. Above approximately 315 nm the influence of clouds on the GOME earthshine measurements and, conse-

quently, on the retrieved ozone profiles is not negligible any more. An exact description of a three-dimensional broken cloud field within a one-dimensional radiative transfer model like GOMETRAN is not possible. Therefore in FURM the following two approximative approaches to deal with clouds were implemented:

1. The CaA (Clouds as Albedo) method consists in replacing the surface albedo used for the radiative transfer calculations by a weighted mean of the surface albedo and the cloud albedo, the weight being the fractional cloud cover.

2. For the CaS (Clouds as bidirectionally reflecting Surfaces) method the radiative transfer calculations are performed both for a cloud free scenario and for a completely cloudy scenario where the cloud is parameterized by a bidirectionally reflecting surface inserted in the model atmosphere at the cloud top height. Then weighted means of the cloud free and cloudy spectra and weighting functions are calculated using the fractional cloud cover as the weight.

The fractional cloud cover of a GOME ground pixel is estimated from the PMD measurements by means of a set of threshold tests [*Kurosu and Burrows,* 1998]. In principle, by combining the fractional cloud cover derived from the PMD measurements and the absorption in the O_2 A and B bands the actual cloud top height can be determined from the GOME measurements. However, so far, only climatological values of the cloud top height derived from the International Satellite Cloud Climatology Project (ISCCP) climatology have been available.

In the CaA approach the increase of the surface albedo leads to an increase of the absolute values of the ozone weighting functions in the troposphere and lower stratosphere, i.e., to an enhanced sensitivity of the measurements to ozone variations in these atmospheric regions. The same effect is observed above the cloud top when looking at the ozone weighting functions for the completely cloudy case in the CaS method. Below the cloud top the ozone weighting functions for the completely cloudy scenario are set to zero since the instrument cannot "see" the atmosphere below the cloud. Here the retrieved ozone profile corresponds to the a priori profile. This implies that for partially cloudy scenes with increasing cloud fraction the retrieval result below the cloud top is increasingly determined by the a priori profile.

Tests with real GOME measurements showed no significant differences between ozone profiles retrieved with the CaA method and profiles retrieved with the CaS method. For the retrieval results presented in section 5 the CaA approach was used.

4.4. Discussion of Weighting Functions

The information which can be extracted from the GOME measurements strongly depends on the wavelength range used. This can be seen from Figure 1, where ozone weighting functions for a typical northern midlatitude winter scenario and a tropical scenario are displayed. Between 290 and 315 nm the peak of the weighting functions is shifted from 40 km to 20 km altitude. The larger the solar zenith angle the more information about the higher altitudes is contained in the measurements. Altitudes above approximately 40 km are accessible if the wavelength range is extended below 290 nm. For wavelengths longer than about 315 nm, where the radiation penetrates deeply into the troposphere, the main peak remains at approximately 20 km altitude and a secondary peak due to multiple-scattering appears in the troposphere. The relative size of this tropospheric peak increases with increasing surface albedo and decreasing solar zenith angle (SZA). Furthermore, since the ozone absorption cross sections in

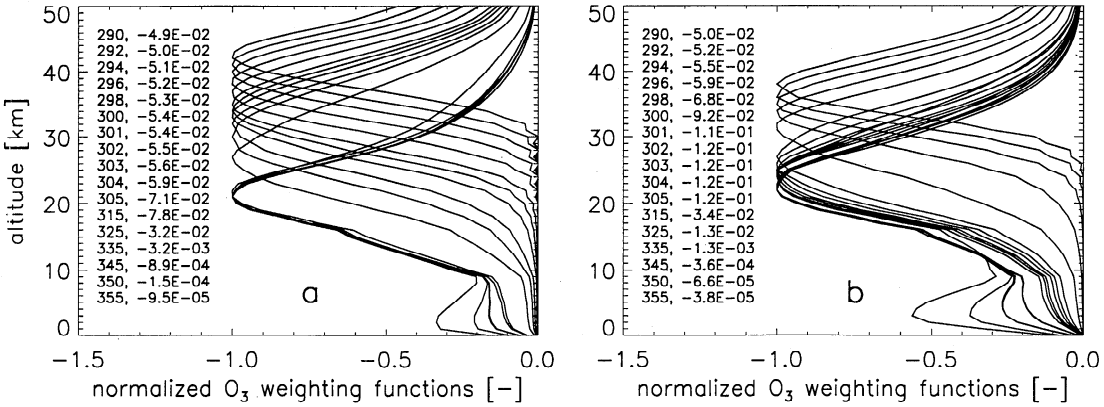

Figure 1. Typical ozone weighting functions for selected wavelengths between 290 and 355 nm. The shortest wavelength is at the top. The weighting functions describe the response of the logarithm of the Sun-normalized radiance to a 100 % increase of ozone in a 1 km layer. For better overview the weighting functions are normalized to their respective maximum value indicated next to the wavelength. (a) Northern midlatitude winter scenario, solar zenith angle SZA=70°, albedo=0.8. (b) Tropical scenario, SZA=20°, albedo=0.05.

the Huggins bands increase with increasing temperature, the tropospheric peak is more pronounced for a warm troposphere than for a cold troposphere. The absolute values of the main peaks strongly decrease with increasing wavelength, reflecting the behavior of the ozone absorption cross sections in this wavelength range.

In this work we restrict ourselves to the wavelength range from 290 to 355 nm, containing typically 580-590 GOME spectral points. One reason for this decision are the strong NOγ emission features corrupting the measurements below 290 nm [*McPeters,* 1989]. These features cannot be simulated with GOMETRAN and therefore adversely affect the retrieval. Between the single NOγ structures there are only small windows of 1-2 nm width, where the shift-and-squeeze correction becomes very difficult. Integration of the single measurements within such a small window does not give satisfying results either. This is due to the fact that the measurement noise, which for wavelengths longer than 290 nm does not exceed 1 %, strongly increases to values of more than 10 % for wavelengths below 290 nm.

Furthermore, there remain unresolved problems with the radiometric calibration of the GOME spectra, particularly at wavelengths between 260 and 290 nm [*Hilsenrath et al.,* 1996]. From the comparison of GOME irradiances with the mean SSBUV-8 irradiance, significant degradation related to the exposure of the optical components of the spectrometer to harmful ultraviolet radiation was observed [*Weber et al.,* 1998]. The current GOME Data Processor makes no correction for the degradation of the GOME optics, which however may be determined inflight using solar, lunar, and linelamp observations. The calibration errors distort the retrieved ozone profiles and appear in the spectral fit residuals as characteristic structures which none of the atmospheric fit parameters can account for. From an analysis of these spectral residuals an empirical "calibration correction function" was derived, which essentially corresponds to a third-order Chebyshev polynomial with different coefficients for channels 1 and 2. Including these coefficients as additional fit parameters clearly improves the retrieval results.

The restriction of the wavelength range to wavelengths longer than 290 nm implies that in the measurements little information is contained about ozone at altitudes above approximately 45 km. Here the retrieved profile essentially tends toward the a priori profile. However, this has little influence on the retrieval results at lower altitudes, because only a small fraction of the total ozone is located above 45 km. Furthermore, the natural variability of ozone is relatively small at high altitudes, so climatological values are sufficiently accurate for our purpose.

As already mentioned in section 4.1, the ozone profile retrieval can be improved by including several non-ozone retrieval parameters. That there is actually information about these parameters in the measurements is demonstrated in Figure 2, where the weighting functions for the pressure, temperature, aerosol, and albedo parameters for the midlatitude scenario and the tropical scenario from Figure 1 are displayed. Over the whole wavelength range the radiance is very sensitive to pressure variations, which lead to proportional changes in the Rayleigh scattering coefficients. For wavelengths shorter than approximately 300 nm, extinction by aerosols and surface reflection are negligible. With increasing wavelength these processes become more and more important, whereas the impact of Rayleigh scattering decreases. For large SZAs the influence of aerosols and the surface sets in at larger wavelengths and for a given scenario is overall smaller than for small SZAs. Between approximately 310 and 330 nm the ozone Huggins structures are clearly visible in the pressure, aerosol, and albedo weighting functions. Since the albedo and the aerosol weighting functions display a similar spectral behavior, the corresponding parameters show a relatively strong correlation. Thus one should be careful with the physical interpretation of the corresponding fit results. Temperature variations influence both the Rayleigh scattering coefficients and the ozone absorption cross sections. Consequently, both signatures can be distinguished in the corresponding weighting functions. To retrieve these "scalar" parameters, the upper boundary of the spectral range used for the retrievals has to be set at large enough wavelengths for the radiation to penetrate down to the Earth surface even for large solar zenith angles. From studies with real and synthetic measurements it was found that 350-355 nm is a suitable value.

4.5. Characterization of the Retrieval

A quantity frequently used to characterize the impact of the true state $\mathbf{x}$ on the retrieved state $\hat{\mathbf{x}}$ is the averaging kernel matrix $\hat{\mathbf{A}}$, which is defined as

$$\hat{\mathbf{A}} = \frac{\partial \hat{\mathbf{x}}}{\partial \mathbf{x}}. \tag{15}$$

For the optimal estimation method, $\hat{\mathbf{A}}$ has the following algebraic form [*Rodgers,* 1990]:

$$\hat{\mathbf{A}} = (\hat{\mathbf{K}}^T \mathbf{S}_\mathbf{y}^{-1} \hat{\mathbf{K}} + \mathbf{S}_a^{-1})^{-1} \hat{\mathbf{K}}^T \mathbf{S}_\mathbf{y}^{-1} \hat{\mathbf{K}}. \tag{16}$$

Using this expression, the retrieval solution can be approximated by

$$\hat{\mathbf{x}} = \mathbf{x}_a + \hat{\mathbf{A}}(\mathbf{x} - \mathbf{x}_a); \tag{17}$$

that is, if the state vector is a profile, the retrieved value at a given altitude can be expressed as the sum of the a priori value at the respective altitude and of the deviation of the true profile from the a priori profile smoothed with the associated row of the averaging kernel matrix.

For an ideal observing system, $\hat{\mathbf{A}}$ is a unit matrix. In reality, the rows of $\hat{\mathbf{A}}$ are peaked functions with a finite width, which can be regarded as a measure of the vertical resolution of the retrieved profile. As an example,

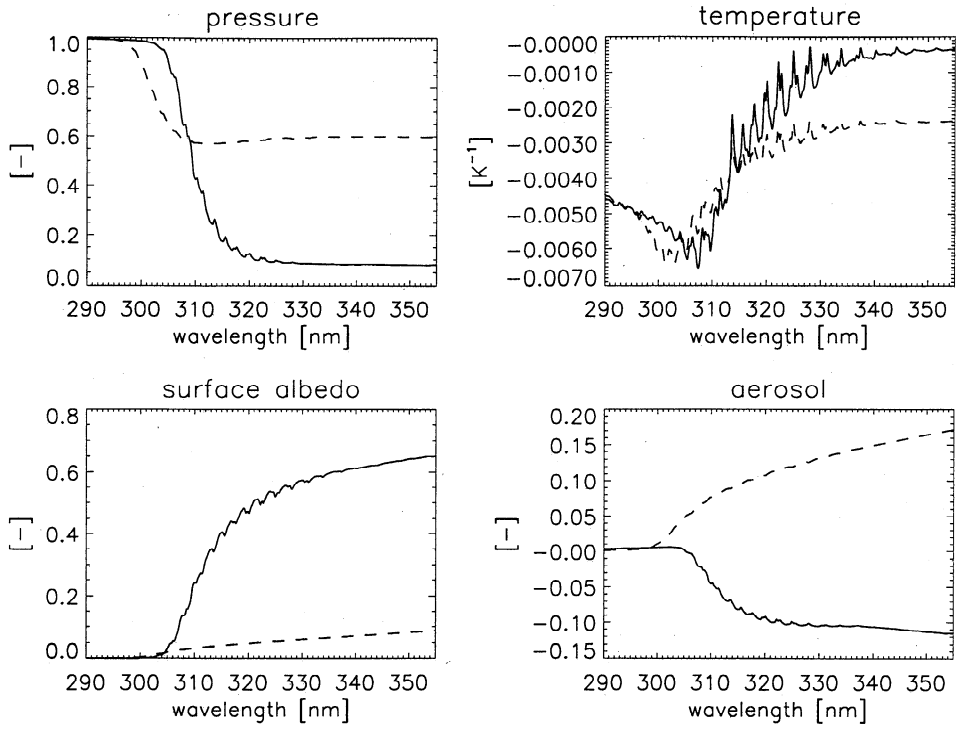

Figure 2. Weighting functions for pressure, temperature, albedo, and aerosol. The weighting functions describe the sensitivity of the logarithm of the Sun-normalized radiance to a 100% increase of the associated parameter in the case of pressure, aerosol, and surface albedo, and to a 1 K increase in the case of temperature. The solid line is for the same scenario as in Figure 1a; the dashed line is for the same scenario as in Figure 1b.

in Figure 3 typical averaging kernels for selected altitudes are displayed for the midlatitude winter scenario and the tropical scenario used to generate the weighting functions in Figure 1. For each averaging kernel its nominal altitude and the actual altitude of the peak maximum are indicated. Between 20 and 35 km the nominal and the actual altitude of the maximum agree very well, and the full width at half maximum (FWHM) of the peak lies between 7 and 9 km. In this height range the retrieved profiles are most accurate and have the best vertical resolution. However, one should not ignore the negative secondary maxima, indicating an anticorrelation between the ozone content at the height of interest and the ozone values at more or less distant altitudes. This observation has to be kept in mind when using the FWHM of the main peak as a measure of the vertical resolution of the retrieved profiles. Below 20 km and above 35 km the actual altitude of the peak maximum does not coincide with its nominal altitude any more, and the FWHM increases to 10 km and

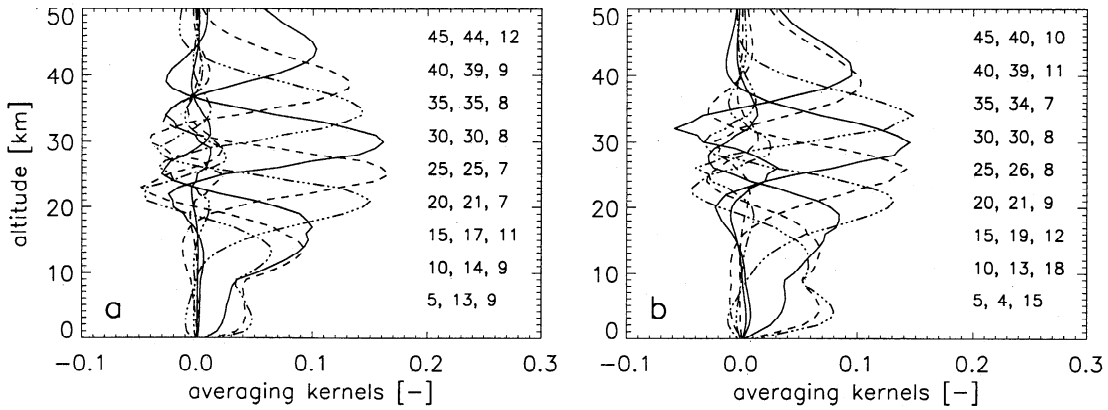

Figure 3. Typical Global Ozone Monitoring Experiment (GOME) averaging kernels for selected altitudes. Atmospheric scenario, SZA, and wavelength range are the same as in Figures 1a and 1b. For each averaging kernel the nominal and the actual height of its maximum and the FWHM of the main peak are indicated.

more. The shape of the averaging kernels suggests that in the lower stratosphere ozone subcolumn amounts can be retrieved. These are of great scientific interest, since they are thought to be suitable early indicators of the healing of the Antarctic ozone hole [*Hofmann*, 1996]. Although the measurements indubitably contain information about the tropospheric ozone content, the corresponding averaging kernels indicate that the retrieved tropospheric ozone concentrations are strongly influenced by the ozone content in the lower stratosphere. How well the variations of the tropospheric and lower stratospheric ozone subcolumn amounts can actually be captured by GOME is discussed in section 5.2.1.

Another informative quantity are the eigenvectors and eigenvalues of the information matrix used in the expansion in (9). The eigenvectors represent independent structures in the ozone profile which can be retrieved from the measurement. All other structures are either linear combinations of these eigenvectors, or disappear in the measurement noise, or cannot be resolved due to the limited vertical resolution of the observing system. The eigenvalues are a measure for the sensitivity of the measurement system to the corresponding ozone variations. Figure 4 shows the eigenvectors and eigenvalues for the same conditions as in Figure 3.

4.6. Error Estimates for GOME Ozone Profiles

Errors in the retrieved ozone profiles result from three independent error sources: measurement errors, errors due to the limited vertical resolution of the observing system ("smoothing error"), and "forward model errors". The latter may be due to the approximative treatment of physical processes in the model and to errors on model parameters (e.g., trace gas cross sections).

Under the assumption that the measurement error is purely random, the sum of measurement error and smoothing error is described by the solution error covariance matrix $\hat{\mathbf{S}}$ (equation (2)). The retrieval errors for the single elements of the state vector are correlated. Since correlated errors are rather difficult to visualize, it is common practice to use the solution standard deviations, i.e., the square roots of the diagonal elements of $\hat{\mathbf{S}}$, to assign error bars to the solution. However, in the case of correlated errors there is actually more information about the state vector than one would have in the case of uncorrelated errors.

Typical profiles of the solution standard deviation and the respective contributions of measurement noise and smoothing error in fractions of the a priori standard deviation are displayed in Figure 5. The smaller the ratio of the solution standard deviation and the a priori standard deviation, the more the knowledge about the atmospheric state has been improved by the measurement (see also (6)). For example, in Figure 5a the ratio is below 0.6 between approximately 11 and 42 km altitude; that is, in this altitude range the measurement considerably improves the knowledge about the ozone distribution compared to the a priori statistics. Below and above this height range the ratio slowly tends toward 1 and the information gain from the measurement decreases.

Typical ranges of the retrieval error for six ozone subcolumn amounts between 0 and 50 km altitude are given in Table 2. The layer boundaries were selected to reflect the vertical resolution of the retrieved profiles. The solution covariance matrix for the ozone subcolumn amounts is given by the transformation of the original solution covariance matrix $\hat{\mathbf{S}}$ according to $\mathbf{T}^T\hat{\mathbf{S}}\mathbf{T}$, where the matrix $\mathbf{T}$ represents the integration operator. For many scientific applications ozone subcolumn amounts with their respective errors may be more useful than the high-resolution ozone profiles. However, one should not forget that the retrieval result in the proper sense is the ozone profile on the high-resolution altitude grid used in the forward calculations to reproduce the measurement to within measurement error.

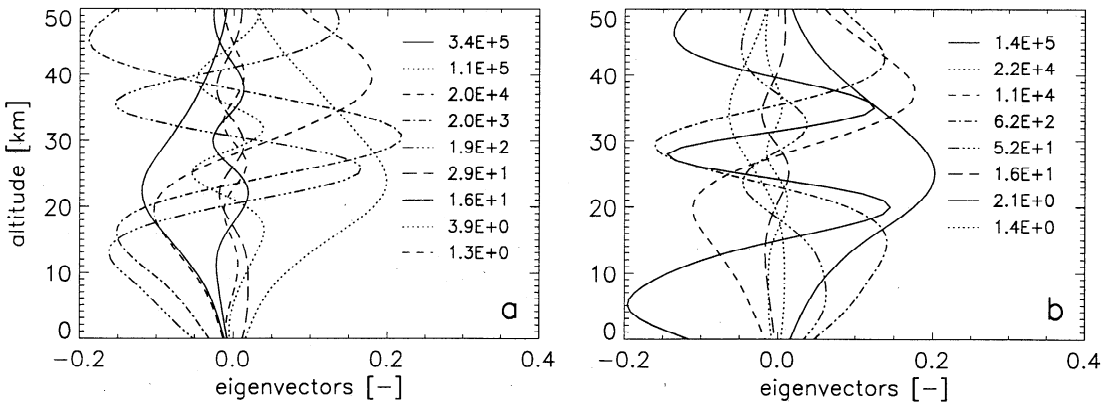

Figure 4. Eigenvectors of the Kozlov information matrix with eigenvalues larger than 1. Atmospheric scenario, SZA, and wavelength range are the same as in Figures 1a and 1b. For each eigenvector the corresponding eigenvalue is given. The higher eigenvectors generally show more oscillations.

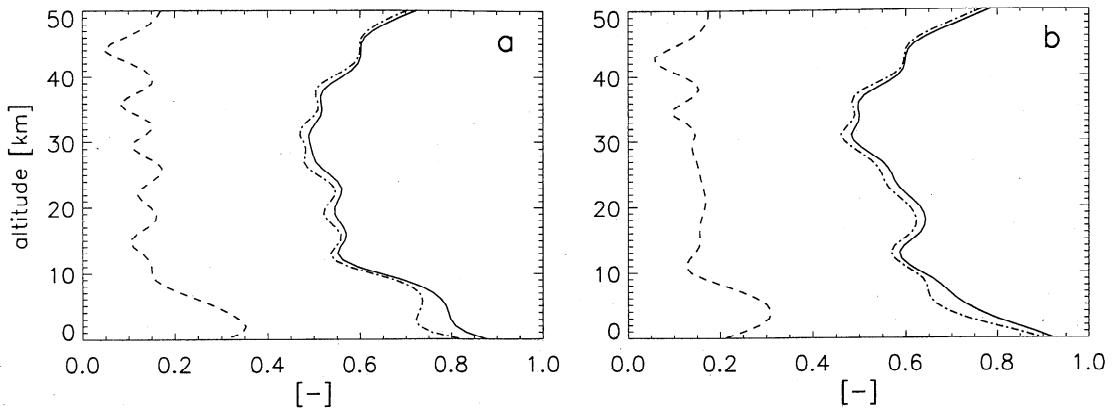

Figure 5. Solution standard deviation in fractions of the a priori standard deviation (solid line) and the contributions from measurement noise (dashed line) and smoothing error (dashed-dotted line). Atmospheric scenario, SZA, and wavelength range are the same as in Figures 1a and 1b.

In addition to the random noise the GOME measurements are corrupted by nonnegligible systematic errors. These errors are partly corrected for by the calibration correction function included in the retrieval process. Remaining effects are difficult to quantify. This also holds for the forward model errors, the most important contributions being the simplified treatment of clouds and the fact that GOMETRAN is a scalar RTM. The latter means that GOMETRAN, as most RTMs, does not solve the complete vector radiative transfer equation (RTE) but the simpler scalar RTE, thereby neglecting the polarization state of the radiation. This restriction affects multiply scattered radiation and can cause radiance errors of several percent with respect to the accurate vector treatment [*Lacis et al.*, 1998; *Mishchenko et al.*, 1994]. Sensitivity tests with synthetic spectra simulated with the radiative transfer model DAK [*de Haan et al.*, 1987; *Stammes et al.*, 1989], which solves the complete vector RTE, showed that the profile error due to the neglect of polarization in GOMETRAN strongly depends on the solar zenith angle and varies from $\pm 1\,\%$ to $\pm 5\,\%$. The net effect of the above mentioned error sources on the retrieved ozone profiles depends on the atmospheric state and measurement geometry and varies with altitude. This makes general statements on its size very difficult. In particular, the error due to the approximative treatment of clouds cannot be estimated with sensitivity studies since an accurate simulation of broken cloud cover is not possible with one-dimensional radiative transfer models like GOMETRAN.

However, empirical estimates of the total profile error can be derived from comparisons of GOME ozone profiles with independent measurements with known uncertainties.

Table 2. Typical Single Retrieval 1σ Error Ranges for GOME Ozone Subcolumn Amounts

Layer Boundaries, km	Error Range, %
0–10	15–20
10–20	6–8
20–27	4–6
27–33	6–8
33–40	6–8
40–50	8–12

5. Comparison With Ozonesonde Measurements

In this section, GOME ozone profiles are validated by comparing them to coincident ozonesonde measurements. The ozonesonde measurements were taken from the NADIR data center at the Norwegian Institute for Air Research (NILU). The sonde stations were selected to represent a good meridional cross section of northern and central Europe. To investigate how well the seasonal ozone variations are captured by GOME, the time period from July 1996 to June 1997 was chosen for the comparison. Only sonde measurements performed on the same day as the GOME overpass were considered. Furthermore, the sonde should have reached at least 30 km altitude, and the center of the GOME ground pixel should be within 500 km from the sonde station (300 km for Ny-Ålesund). Table 3 gives a summary of the sonde measurements used in the comparison.

5.1. Comparison of FURM and DOAS Ozone Total Columns

Before comparing the GOME and the sonde profiles it is interesting to compare the ozone total column amounts obtained by integrating the FURM ozone profiles and the ozone column amounts derived with the Differential Optical Absorption Spectroscopy (DOAS) method. Details of the DOAS method and its application to GOME measurements can be found in the work of *Burrows et al.* [1999b]. The DOAS algorithm and the FURM algorithm are independent methods for the

Table 3. Summary of Coincident Sonde Measurements

Station	Sonde Type	Geolocation	Number
Ny-Ålesund	ECC	78.93°N, 11.95°E	32
Sodankylä	ECC	67.24°N, 26.36°E	19
Lerwick	ECC	60.13°N, 1.18°W	24
Hohenpeißenberg	Brewer-Mast	47.48°N, 11.01°E	49
Payerne	Brewer-Mast	46.80°N, 6.95°E	73

retrieval of ozone total columns from GOME spectra. Since the respective retrieval results are based on measurements performed by the same instrument viewing the same air mass, differences between the results can be exclusively attributed to differences in the retrieval algorithms.

While the FURM method is based on absolutely calibrated measurements covering a broad spectral range, the DOAS method uses differential spectral structures in relatively small spectral windows. Within these small spectral windows, broadband spectral structures can be easily taken into account by low-order polynomials. Therefore the DOAS results are much less affected by broadband calibration errors or by atmospheric parameters with broadband spectral structures (e.g., aerosol, surface albedo, clouds) than the FURM results. An extensive pole-to-pole validation of the GOME DOAS total ozone values with the SAOZ ground-based network was performed by *Lambert et al.* [1997a]. For SZAs below 60° the GOME and the SAOZ total columns agree to within ±4 %. Similar results were obtained in a comparison of the GOME DOAS total ozone with Dobson and Brewer observations at the NDSC/Alpine stations [*Lambert et al.*, 1997b]. Thus for SZAs below 60° the DOAS total columns can be considered a good reference for the comparison with the corresponding FURM results. At SZAs larger than about 60° the GOME total ozone values are systematically lower than the correlative measurements. This may be explained by known problems with the air mass factors at high SZAs affecting the operational DOAS results but not the FURM retrievals.

The comparison between the FURM and the DOAS results is overall consistent with these observations. As can be seen from Figure 6, for all five stations the seasonal variations of total ozone derived with the FURM and the DOAS algorithm are very similar. The best agreement is found at Hohenpeißenberg and Payerne, where the mean relative difference between the FURM and the DOAS total columns is below 0.1 %. At Lerwick and Sodankylä a mean relative difference of approximately 2 % is observed, the FURM algorithm providing the higher values. At Ny-Ålesund the FURM total columns are, on the average, 5 % higher than the corresponding DOAS results. Thus at higher SZAs the FURM total column amounts appear to agree better with the SAOZ measurements than the operational DOAS total column amounts.

5.2. Intercomparison of Ozone Profiles

When comparing GOME ozone profiles with ozonesonde measurements, the different vertical resolutions of both sensors have to be taken into account. In particular, in the tropopause region and lower stratosphere the rapid changes of ozone with altitude seen by the sondes cannot be resolved by GOME. Therefore, for a quantitative comparison, the sonde measurements have to be degraded to the vertical resolution of the GOME profiles. In the following subsections, three intercomparison procedures are presented, namely, the comparison of ozone subcolumn amounts, the comparison of the GOME ozone profiles with sonde profiles which were smoothed with the GOME averaging kernels, and the comparison between monthly mean GOME and sonde profiles.

5.2.1. Comparison of ozone subcolumn amounts. The definition of layer boundaries for the calculation of ozone subcolumn amounts is somewhat arbitrary, and a given set of boundaries may not be adequate for all atmospheric conditions. To facilitate matters, in this comparison, three atmospheric layers ranging from 0 to 10 km, from 10 to 20 km, and from 20 to 30 km altitude were defined, which may be regarded as representative of the troposphere, lower and middle stratosphere, respectively. The layer thickness approximately corresponds to the vertical resolution of the GOME ozone profiles.

In Figure 7 the ozone subcolumn amounts as derived from the GOME and the sonde profiles are displayed. For comparison also the a priori subcolumn amounts are given. For all stations the seasonal ozone variations in the lower and middle stratosphere detected by GOME and the ozonesondes are very similar. The mean relative differences and the root-mean-square (RMS) of the relative differences between the GOME and the sonde measurements and between the climatology and the sonde measurements are summarized in Table 4. In the troposphere (0-10 km) the RMS between the GOME and the sonde subcolumns varies between 21 and 24 % and is slightly smaller than the RMS between the a priori and the sonde subcolumns. For all stations except Ny-Ålesund the mean relative difference between the GOME and the sonde results is significantly smaller than the mean relative difference between the a priori and the sonde values. In the lower stratosphere (10-20 km) for Lerwick, Hohenpeißenberg, and Payerne the RMS between the GOME and the sonde subcolumns

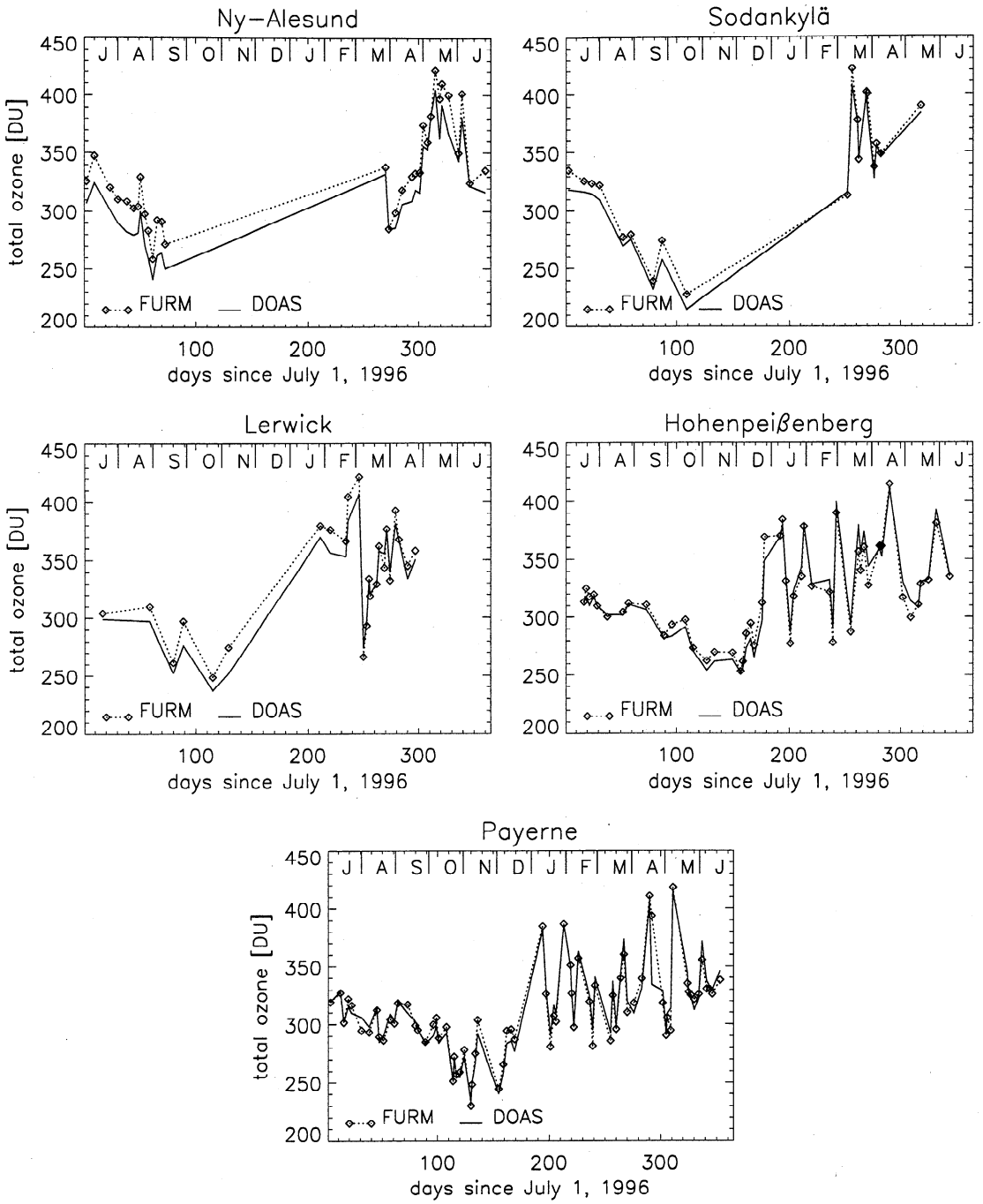

Figure 6. GOME ozone total columns calculated by integrating the ozone profiles retrieved with the Full Retrieval Method (FURM) algorithm and derived with the operational Differential Optical Absorption Spectroscopy (DOAS) algorithm.

is almost a factor of 3 smaller than the RMS between the a priori and the sonde subcolumns. For Ny-Ålesund and Sodankylä the RMS is reduced by a factor of 1.7 and 2.3, respectively. These results demonstrate that reliable results can be obtained even if the actual ozone distribution differs strongly from the a priori values (see Figure 7). On the average the GOME subcolumns are 7-10 % higher than the sonde results. In the middle stratosphere (20-30 km) for all stations except Lerwick a relatively small RMS of 7-8 % and a small relative deviation of less than ±5 % between the GOME and the sonde subcolumns is observed. Apart from a few exceptions the results of the statistical evaluation of the comparison are rather similar for all stations, which allows their generalization for northern midlatitudes.

The root-mean-square scatter of the differences between the GOME and the sonde subcolumns might seem relatively large compared to the 1σ errors given in Table 2, even if the uncertainties of the sonde measurements are taken into account. However, because of

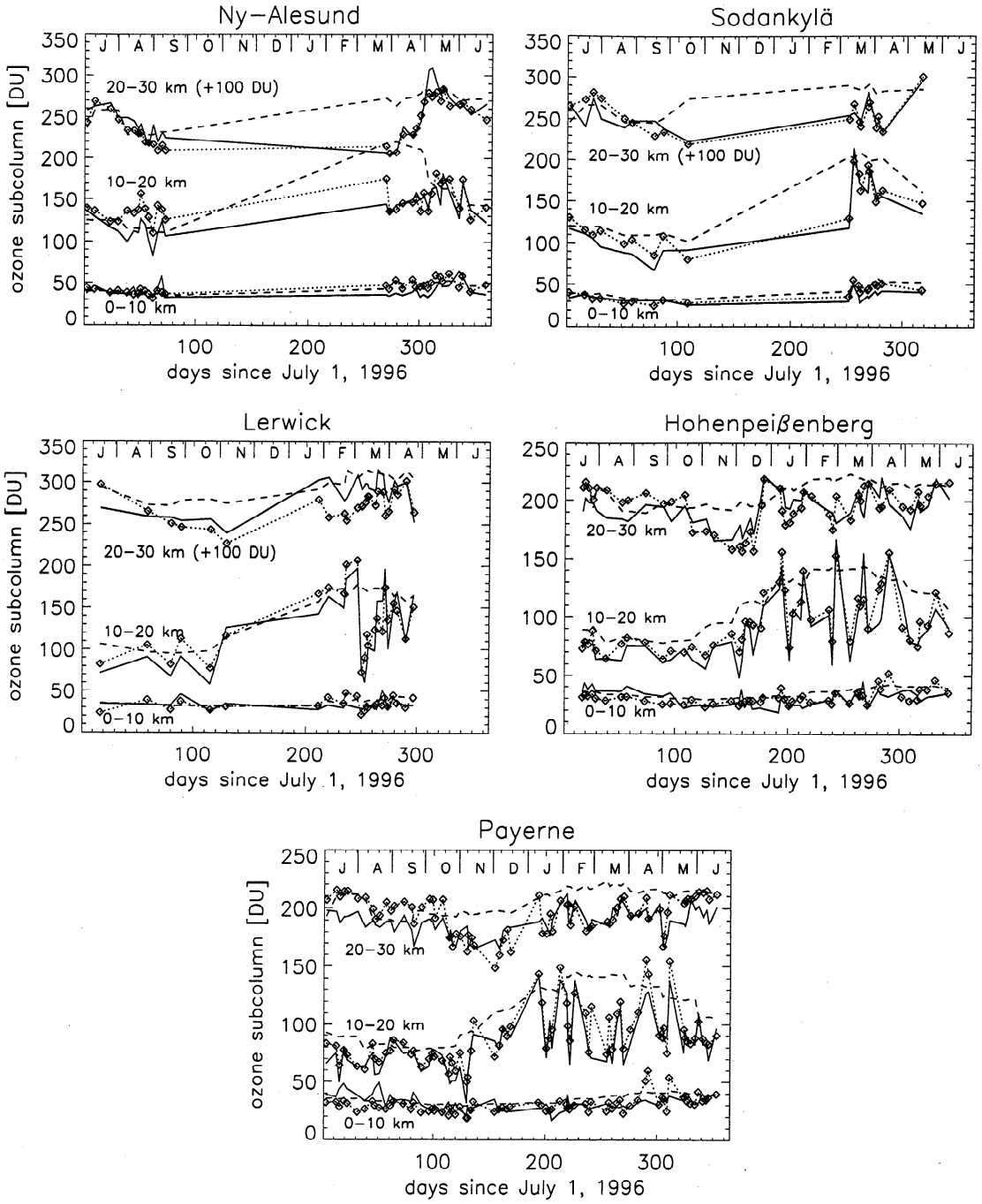

Figure 7. GOME (dotted line with symbols), sonde (solid line), and climatology (dashed line) ozone subcolumn amounts for three atmospheric layers: 0-10 km, 10-20 km, 20-30 km. For Ny-Ålesund, Sodanklyä, and Lerwick the subcolumn amounts of the topmost layer were shifted by +100 Dobson units (DU).

the large GOME ground pixel size of $960 \times 100\,\mathrm{km}^2$ and the time lag of up to several hours between the sonde launches and the GOME overpasses, GOME and the sondes do not view exactly the same air mass. This deteriorates the comparison results, particularly in regions with large horizontal and temporal ozone gradients, e.g., close to the boundary of the polar vortex. Furthermore, in Table 2, calibration errors and forward model errors are not taken into account. Therefore the actual scatter in the comparison is expected to be larger than predicted by theoretical error analysis.

5.2.2. Comparison of GOME profiles with smoothed sonde profiles. A method of removing the influence of different vertical resolutions and the bias introduced by the use of a priori information from the comparison can be derived from (17). Replacing the true ozone profile $\mathbf{x}$ by the high-resolution sonde profile $\mathbf{x}_s$ yields

Table 4. Mean Relative Differences and RMS of Relative Differences Between GOME and Sonde Ozone Subcolumn Amounts (row 1 for each station) and Between a Priori and Sonde Ozone Subcolumn Amounts (row 2)

	Layer 1 (0-10 km)		Layer 2 (10-20 km)		Layer 3 (20-30 km)	
	Mean Difference	RMS	Mean Difference	RMS	Mean Difference	RMS
Ny-Ålesund	12.8	23.2	9.9	15.9	-4.3	7.7
	11.0	25.1	15.2	26.3	8.0	22.2
Sodankylä	11.3	19.6	7.0	12.8	0.7	8.0
	22.2	27.9	23.1	29.5	12.9	19.3
Lerwick	3.0	21.2	10.0	21.1	-7.3	10.9
	13.6	23.3	36.4	61.6	9.2	12.7
Hohenpeißenberg	4.5	24.2	8.6	16.7	0.4	6.9
	18.2	29.5	33.8	48.6	7.1	10.6
Payerne	-3.0	23.2	8.5	17.6	3.1	7.0
	12.5	23.9	38.2	52.5	9.7	11.5

Values given in percent.

$$\mathbf{x}_c = \mathbf{x}_a + \hat{\mathbf{A}}(\mathbf{x}_s - \mathbf{x}_a), \tag{18}$$

where $\mathbf{x}_c$ is the sonde profile convoluted with the GOME averaging kernels. In the absence of calibration and forward model errors, $\mathbf{x}_c$ corresponds to what the GOME retrieval would be if $\mathbf{x}_s$ were the true profile. Thus the comparison between the convoluted sonde profiles and the GOME profiles is an excellent tool to identify systematic differences between the two data sets. This approach was first suggested by *Connor et al.* [1991].

Before being convoluted with the GOME averaging kernels the sonde profiles have to be extended with climatological ozone profiles to cover the whole GOME altitude range. To reduce the effect of this extension, the convoluted sonde profiles are truncated at 30 km altitude. The single profile comparisons displayed in Figure 8 illustrate the procedure. As can be seen, the dynamically induced secondary ozone maxima in the lower stratosphere cannot be captured by GOME.

As a measure of a possible bias between the GOME and the sonde profiles, Figure 9 shows the mean relative differences between the GOME and the smoothed sonde profiles. Over almost the entire altitude range the differences are below 10 % with GOME yielding the higher ozone concentrations. The agreement is best at Hohenpeißenberg and Payerne (better than 8 % over the entire altitude range), which may in part be due to the fact that for these two stations the Dobson correction was applied to the sonde profiles.

Also displayed in Figure 9 are the root-mean-squares of the relative differences, which can be regarded as a measure of the scatter of the GOME measurements about the sonde measurements. Generally, the RMS is largest in the tropopause and lowermost stratosphere, where the natural ozone variability is largest. For all stations the RMS reaches its maximum of the order of 15-20 % at about 10-13 km altitude. Above 18 km altitude the RMS decreases to about 10 % for all stations.

5.2.3. Comparison of monthly mean ozone profiles. A good way of investigating how well the seasonal ozone variations are detected by GOME is to compare monthly means of the coincident sonde and GOME profiles. The averaging of the sonde profiles leads to a certain smoothing of the vertical structures.

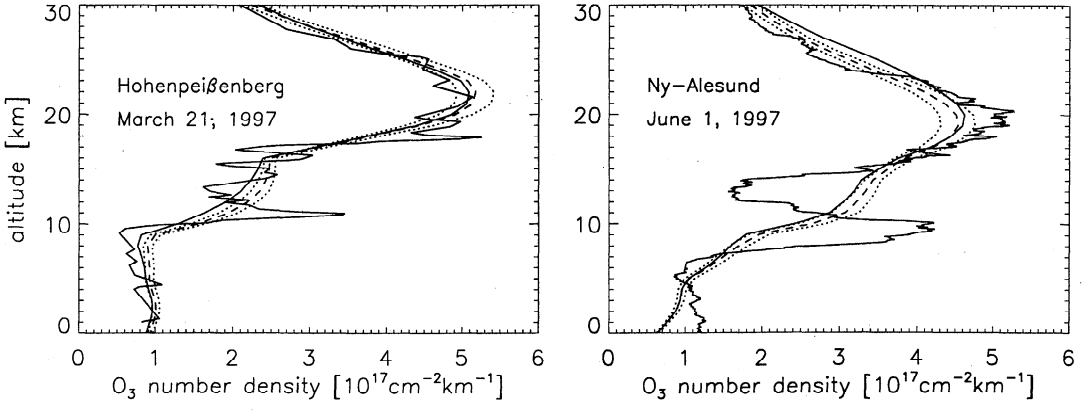

Figure 8. Single ozone profile comparisons. The highly structured solid line is the original sonde measurement; the smooth solid line is the same profile after convolution with the GOME averaging kernels. The dashed line is the GOME retrieval. The dotted lines indicate the 1σ error due to measurement noise.

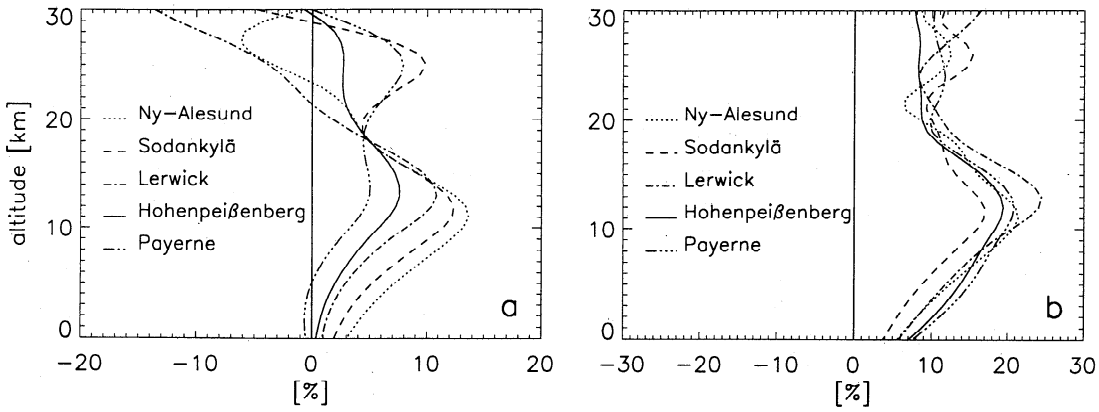

Figure 9. (a) Mean relative differences between the GOME ozone profiles and the convoluted sonde profiles. (b) RMS of the relative differences between the GOME profiles and the convoluted sonde profiles.

However, unlike in the comparison with sonde profiles convoluted with the GOME averaging kernels, the bias introduced in the GOME profiles by the use of a priori information is not removed from the comparison.

Figure 10 shows the mean profiles for March 1997 in Sodankylä, Lerwick, Hohenpeißenberg, and Payerne. Above approximately 15 km altitude the sonde and the GOME profiles agree to within ±10 %. In the tropopause region the different vertical resolutions lead to larger deviations. Strikingly, for all four stations the lower stratospheric ozone concentrations in March 1997 are much lower than the climatological a priori values based on the years 1980-1991. The total columns are 15-20 % below the climatological values. To a large ex-

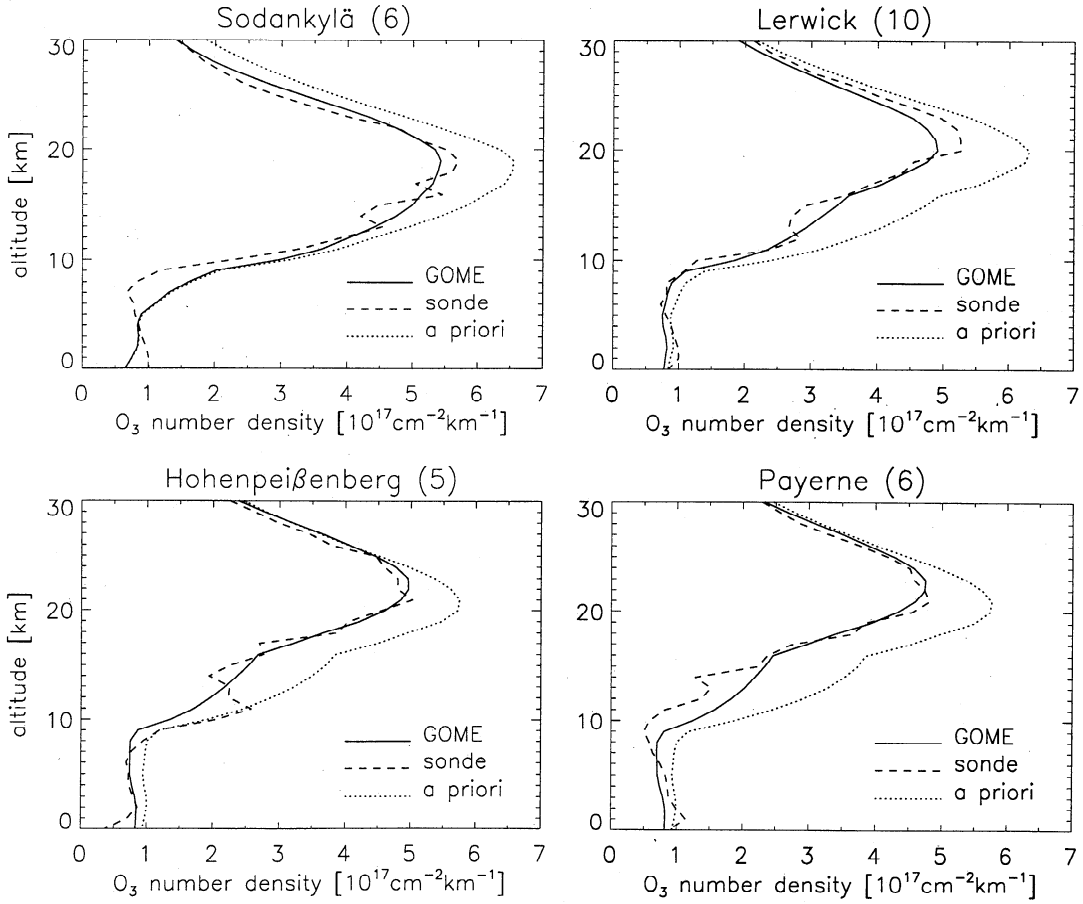

Figure 10. Monthly means of the coincident GOME and sonde profiles for March 1997. For comparison the climatological a priori profile is also displayed. In the plot titles the number of profiles used to derive the monthly mean profile is indicated.

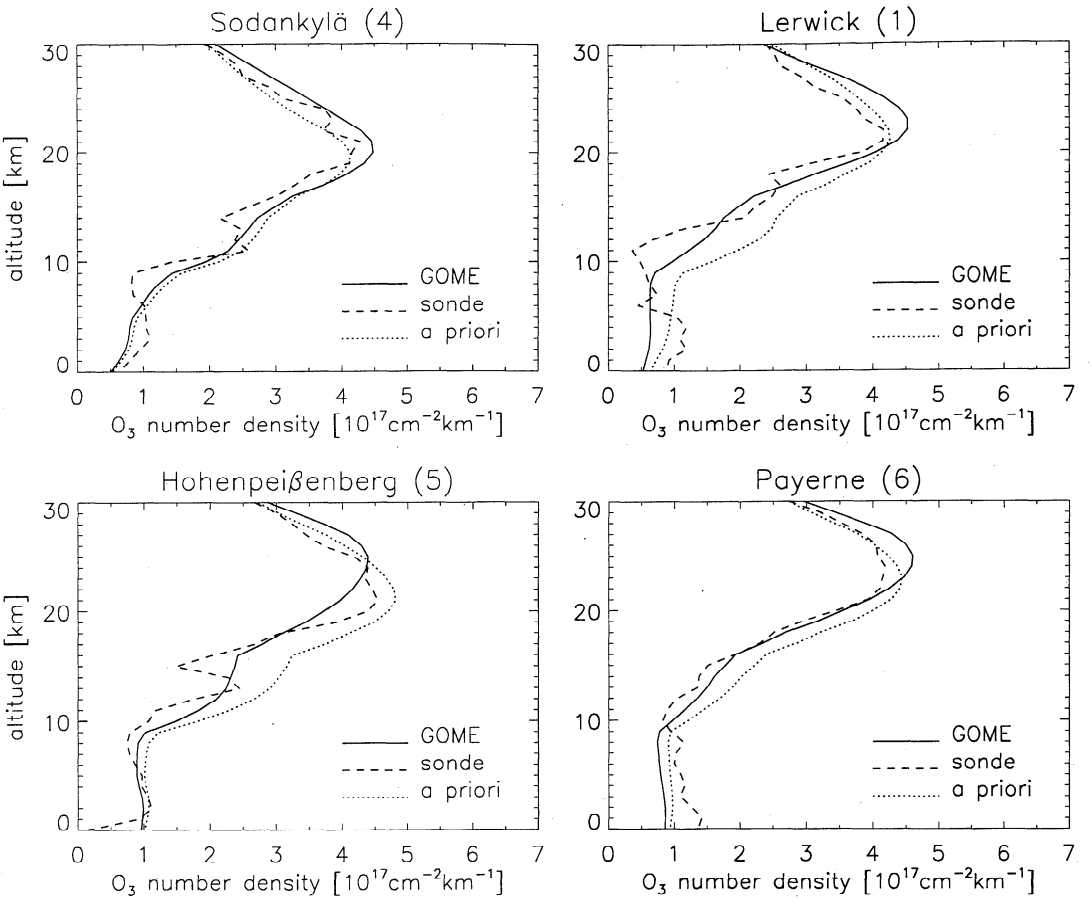

Figure 11. As Figure 10 for July 1996.

tent, these low ozone values are due to the particular dynamical situation in March 1997, which was characterized by frequent intrusions of subtropical air into midlatitudes [e.g., *Entzian and Peters,* 1998; *O'Connor and Vaughan,* 1998].

In Figure 11 the mean profiles for July 1996 are displayed. Above the ozone maximum the GOME ozone concentrations tend to be higher than the sonde values. This observation is consistent with Figure 7, where in the summer half of the year the GOME subcolumn amounts between 20 and 30 km altitude are systematically higher than the corresponding sonde values. The most probable cause for these discrepancies between the GOME and the sonde measurements are errors in the absolute radiometric calibration of the GOME spectra. However, more detailed investigations are needed to draw a final conclusion.

6. Summary

The FURM algorithm for the derivation of ozone profiles from GOME satellite measurements has been presented. The retrieval method is based on the optimal estimation approach and explicitly considers the information content of the measurement. An essential part of the retrieval algorithm is the radiative transfer model GOMETRAN used for the calculation of radiances and weighting functions. The FURM results are reported as high-resolution ozone profiles between 0 km and 80 km altitude. For scientific applications the integration of these high-resolution profiles to layers reflecting the actual vertical resolution of the profiles is recommended.

To assess the quality of the GOME ozone profiles, a comparison with 197 coincident ozonesonde measurements from five European stations covering a broad range of latitudes was performed. The measurement period was selected to span one entire year. Taking into account the known uncertainties of the sonde and the GOME measurements and the imperfect temporal and spatial coincidence the results of the intercomparison are overall very satisfying. In particular, it was demonstrated that ozone subcolumn amounts for the lower stratosphere can be retrieved.

The retrieved ozone profiles are very sensitive to the absolute radiometric calibration of the GOME spectra. Therefore further improvements are expected with future updates of the calibration. In addition, a more accurate calibration of GOME channel-3 data will permit the use of the ozone Chappuis bands in the retrieval, which under certain conditions can improve the retrieval results in the troposphere [*de Beek,* 1998]. Recently, the boundary between GOME channels 1A and 1B has been shifted to 283 nm to enable the retrieval of ozone profiles with a higher horizontal resolution ($320 \times 40\,km^2$). This,

in conjunction with a more sophisticated treatment of cloudy scenes foreseen for the next version of the algorithm, is expected to further improve the quality of the GOME ozone profiles, in particular in the troposphere.

A first scientific application of the FURM algorithm was the derivation of ozone vertical distributions from GOME data in the northern hemisphere during the Arctic winters 1996/1997 and 1997/1998 [*Bramstedt et al.*, 1998; *Eichmann et al.*, 1998].

Acknowledgments. We thank K. Bramstedt for his support with the extraction and preparation of the GOME level-1 data and M. Buchwitz for keeping GOMETRAN up to date. The ozonesonde measurements were provided by H. Gernandt (AWI), E. Kyrö (FMI), R. J. Shearman (UKMO), H. Claude (DWD), and P. Viatte and B. Henchoz (SMI). The NMC analyses were provided by M. Schoeberl, P. Newman, R. N. Nagatani, and L. Lait and accessed via the NASA Goddard AutoMailer.

References

Bates, D. R., Rayleigh scattering by air, *Planet. Space Sci., 32,* 785-790, 1984.

Bhartia, P. K., R. D. McPeters, C. L. Mateer, L. E. Flynn, and C. Wellemeyer, Algorithm for the estimation of vertical ozone profiles from the backscattered ultraviolet technique, *J. Geophys. Res., 101,* 18,793-18,806, 1996.

Bramstedt, K., K.-U. Eichmann, M. Weber, V. Rozanov, R. Hoogen, R. de Beek, M. Buchwitz, T. Kurosu, and J. P. Burrows, Ozone profiles from GOME satellite data – Part II: First results from the arctic winter campaign, *Eur. Comm. Air Pollut. Rep., 66,* 189-192, 1998.

Bucholtz, A., Rayleigh-scattering calculations for the terrestrial atmosphere, *Appl. Opt., 34,* 2765-2773, 1995.

Burrows, J. P., W. Schneider, and K. V. Chance, GOME and SCIAMACHY: Remote sensing of stratospheric and tropospheric gases, *Eur. Comm. Air Pollut. Rep., 34,* 99-102, 1991.

Burrows, J. P., E. Hölzle, A. P. H. Goede, H. Visser, and W. Fricke, SCIAMACHY - Scanning Imaging Absorption Spectrometer for Atmospheric Chartography, *Acta Astronaut., 35,* 445-451, 1995.

Burrows, J. P., A. Dehn, B. Deters, S. Himmelmann, A. Richter, S. Voigt, and J. Orphal, Atmospheric remote sensing reference data from GOME – Part 1: Temperature dependent absorption cross sections of NO_2 in the 231-794 nm range, *J. Quant. Spectrosc. Radiat. Transfer, 60,* 1025-1031, 1998.

Burrows, J. P., A. Richter, A. Dehn, B. Deters, S. Himmelmann, S. Voigt, and J. Orphal, Atmospheric remote sensing reference data from GOME – Part 2: Temperature dependent cross sections of O_3 in the 231-794 nm range, *J. Quant. Spectrosc. Radiat. Transfer,* in press, 1999a.

Burrows, J. P., et al., The Global Ozone Monitoring Experiment (GOME): Mission concept and first scientific results, *J. Atmos. Sci., 56,* 151-175, 1999b.

Connor, B. J., A. Parrish, and J.-J. Tsou, Detection of stratospheric ozone trends by ground-based microwave observations, *Proc. SPIE, 1491,* 218-230, 1991.

de Beek, R., Bestimmung von Ozonvertikalverteilungen aus Messungen des Satelliteninstruments GOME im ultravioletten und sichtbaren Spektralbereich, 218 pp., PhD thesis, Univ. Bremen, Germany, 1998.

de Haan, J. F., P. B. Bosma, and J. W. Hovenier, The adding method for multiple scattering calculations of polarized light, *Astron. Astrophys., 183,* 371-391, 1987.

Derrien, M., Influence of the size of field of view on the contamination by clouds, *Tech. Rep. contract 9239,* Météo-France, Toulouse, France, 1992.

Deutsche Forschungsanst. für Luft- und Raumfahrt (DLR), GOME level 0 to 1 algorithms description, *Tech. Note ER-TN-DLR-GO-0022,,* Dt. Forschungsanst. für Luft- und Raumfahrt DLR/DFD, Oberpfaffenhofen, Germany, 1996.

Eichmann, K.-U., M. Weber, K. Bramstedt, R. Hoogen, V. Rozanov, and J. P. Burrows, Ozone profile distributions in the Arctic from GOME satellite observations during spring 1997 and 1998, *Proc. SPIE, 3495,* 357-366, 1998.

Entzian, G., and D. Peters, Dynamically induced zonal asymmetric low ozone values in the North Atlantic-European region during March 1997, *Eur. Comm. Air Pollut. Rep., 66,* 36-39, 1998.

European Space Agency (ESA), GOME users manual, *ESA SP-1182,* Eur. Space Agency, ESA/ESTEC, Nordwijk, Netherlands, 1995.

Farman, J. C., B. G. Gardiner, and J. D. Shanklin, Large losses of total ozone in Antarctica reveal seasonal ClO_x/NO_x interaction, *Nature, 315,* 207-210, 1985.

Fishman, J., C. E. Watson, J. C. Larsen, and J. A. Logan, Distribution of tropospheric ozone determined from satellite data, *J. Geophys. Res., 95,* 3599-3617, 1990.

Fishman, J., V. G. Brackett, E. V. Browell, and W. B. Grant, Tropospheric ozone derived from TOMS/SBUV measurements during TRACE A, *J. Geophys. Res., 101,* 24,069-24,082, 1996.

Fortuin, J. P. F., An ozone climatology based on ozonesonde measurements, *Sci. Rep. WR 96-07,* 44 pp., Royal Netherlands Met. Inst. (KNMI), de Bilt, Netherlands, 1996.

Fortuin, J. P. F., and H. Kelder, An ozone climatology based on ozonesonde and satellite measurements, *J. Geophys. Res., 103,* 31,709-31,734, 1998.

Grainger, J. F., and J. Ring, Anomalous Fraunhofer line profiles, *Nature, 193,* 762, 1962.

Heath, D. F., C. L. Mateer, and A. J. Krueger, The Nimbus 4 backscattered ultraviolet (BUV) atmospheric ozone experiment – 2 years of operation, *Pure Appl. Geophys., 1238,* 106-108, 1973.

Heath, D. F., A. J. Krueger, H. R. Roeder, and B. D. Henderson, The Solar Backscatter Ultraviolet and Total Ozone Mapping Spectrometer (SBUV/TOMS) for Nimbus G, *Opt. Eng., 14,* 323-331, 1975.

Hilsenrath, E., D. Williams, and J. Frederick, Calibration of long term data sets from operational satellites using the Space Shuttle, *SPIE Proc., 924,* 215-222, 1988.

Hilsenrath, E., J. Gleason, S. Janz, X. Gu, R. P. Cebula, K. Chance, and R. Hoekstra, GOME calibration and validation using backscatter UV techniques, paper presented at the Final Results Workshop of the GOME Geophysical Validation Campaign, Eur. Space Agency, ESA/ESRIN, Frascati, Italy, Jan. 24-26, 1996.

Hofmann, D. J., Recovery of Antarctic ozone hole, *Nature, 384,* 222, 1996.

Kneizys, F. X., E. P. Shettle, L. W. Abreu, J. H. Chetwynd, G. P. Anderson, W. O. Gallery, J. E. A. Selby, and S. A. Clough, Users guide to LOWTRAN 7, *Tech. Rep. AFGL-TR-88-0177,* Air Force Geophys. Lab., Bedford, Mass., 1988.

Kozlov, V., Design of Experiments Related to the Inverse Problem of Mathematical Physics (in Russian), in *Mathematical Theory of Experiment Design,* edited by C. M. Ermakov, pp. 216-246, Nauka, Moscow, 1983.

Kurosu, T., V. V. Rozanov, and J. P. Burrows, Parameterization schemes for terrestrial water clouds in the radiative transfer model GOMETRAN, *J. Geophys. Res., 102,* 21,809-21,823, 1997.

Kurosu, T., and J. P. Burrows, PMD cloud detection algorithm for the GOME instrument – Algorithm description and users manual, *Tech. Rep. 11572/2/95/NL/CN,* Eur. Space Agency, ESA/ESTEC, Noordwijk, Netherlands, 1998.

Lacis, A. A., J. Chowdhary, M. I. Mishchenko, and B. Cairns, Modeling errors in diffuse-sky radiation: Vector vs. scalar treatment, *Geophys. Res. Lett., 25,* 135-138, 1998.

Lambert, J.-C., et al., Pole-to-pole validation of the ERS-2 GOME level 2 products with the SAOZ ground-based network, paper presented at the 3rd ERS Symposium, *ESA SP-414,* pp. 629-636, Eur. Space Agency, ESA/ESTEC, Noordwijk, Netherlands, 1997a.

Lambert, J.-C., et al., Validation of the ERS-2 GOME ozone products with the NDSC/alpine stations, paper presented at the 3rd ERS Symposium, *ESA SP-414,* pp. 729-732, Eur. Space Agency, ESA/ESTEC, Noordwijk, Netherlands, 1997b.

Mateer, C. L., D. F. Heath, and A. J. Krueger, Estimation of total ozone from satellite measurements of backscattered ultraviolet Earth radiance, *J. Atmos. Sci., 28,* 1307-1311, 1971.

McPeters, R. D., Climatology of nitric oxide in the upper stratosphere, mesosphere, and thermosphere: 1979 through 1986, *J. Geophys. Res., 94,* 3461-3472, 1989.

Mishchenko, M. I., A. A. Lacis, and L. D. Travis, Errors induced by the neglect of polarization in radiance calculations for Rayleigh-scattering atmospheres, *J. Quant. Spectrosc. Radiat. Transfer, 51,* 491-510, 1994.

O'Connor, F. M., and G. Vaughan, Irreversible transport of subtropical air into the northern mid-latitude lower stratosphere during March 1997, *Eur. Comm. Air Pollut. Rep., 66,* 54-57, 1998.

Rodgers, C. D., Retrieval of atmospheric temperature and composition from remote measurements of thermal radiation, *Rev. Geophys., 14,* 609-624, 1976.

Rodgers, C. D., Characterization and error analysis of profiles retrieved from remote sounding measurements, *J. Geophys. Res., 95,* 5587-5595, 1990.

Rodgers, C. D., Information content and optimization of high-spectral-resolution measurements, *Proc. SPIE, 2839,* 136-147, 1996.

Rozanov, V. V., D. Diebel, R. J. D. Spurr, and J. P. Burrows, GOMETRAN: A radiative transfer model for the satellite project GOME, the plane-parallel version, *J. Geophys. Res., 102,* 16,683-16,695, 1997.

Rozanov, V. V., T. Kurosu, and J. P. Burrows, Retrieval of atmospheric constituents in the UV-visible: A new quasi-analytical approach for the calculation of weighting functions, *J. Quant. Spectrosc. Radiat. Transfer, 60,* 277-299, 1998.

Shannon, C. E., and W. Weaver, *The Mathematical Theory of Communication,* Univ. of Illinois Press, Urbana, 1949.

Shefov, N. N., Spectroscopic, photoelectric, and radar investigations of aurorae and the nightglow (in Russian), *Izv. Akad. Nauk, 1,* 25, 1959.

Singer, S. F., and R. C. Wentworth, A method for the determination of the vertical ozone distribution from a satellite, *J. Geophys. Res., 62,* 299-308, 1957.

Stammes, P., J. F. de Haan, and J. W. Hovenier, The polarized internal radiation field of a planetary atmosphere, *Astron. Astrophys., 225,* 239-259, 1989.

Suhre, K., J.-P. Cammas, P. Nédelec, R. Rosset, A. Marenco, and H. G. J. Smit, Ozone-rich transients in the upper equatorial Atlantic troposphere, *Nature, 388,* 661-663, 1997.

Vountas, M., V. V. Rozanov, and J. P. Burrows, Ring effect: Impact of rotational Raman scattering on radiative transfer in Earth's atmosphere, *J. Quant. Spectrosc. Radiat. Transfer, 60,* 943-961, 1998.

Weber, M., J. P. Burrows, and R. P. Cebula, GOME solar UV/VIS irradiance measurements between 1995 and 1997 – First results on proxy solar activity studies, *Sol. Phys., 177,* 63-77, 1998.

J. P. Burrows, R. Hoogen, and V. V. Rozanov, Institut für Umweltphysik, Universität Bremen, Postfach 330440, 28334 Bremen, Germany. (e-mail: John.Burrows@iup.physik.uni-bremen.de; Ricarda.Hoogen@iup.physik.uni-bremen.de; Vladimir.Rozanov@iup.physik.uni-bremen.de)

(Received June 30, 1998; revised November 2, 1998; accepted December 9, 1998.)